Chemically assisted femtosecond laser machining for applications in LiNbO[subscript 3] and LiTaO[subscript 3]

Citation: Sivarajah, Prasahnt, Christopher A. Werley, Benjamin K. Ofori-Okai, and Keith A. Nelson. "Chemically Assisted Femtosecond Laser Machining for Applications in LiNbO3 and LiTaO3." Applied Physics A 112, no. 3 (July 6, 2013): 615–622.

As Published: http://dx.doi.org/10.1007/s00339-013-7833-x

Publisher: Springer Berlin Heidelberg

Persistent URL: http://hdl.handle.net/1721.1/103600

Version: Author's final manuscript: final author's manuscript post peer review, without publisher's formatting or copy editing

Applied Physics A:Materials Science & Processing manuscript No.
(will be inserted by the editor)

Chemically Assisted Femtosecond Laser Machining for Applications in $LiNbO_3$ and $LiTaO_3$

Prasahnt Sivarajah · Christopher A. Werley · Benjamin Ofori-Okai · Keith A. Nelson

Received: date / Accepted: date

Abstract We introduce and optimize a fabrication procedure that employs both femtosecond laser machining and hydrofluoric acid etching for cutting holes or voids in slabs of lithium niobate and lithium tantalate. The fabricated structures have 3 μm lateral resolution, a lateral extent of at least several millimeters, and cut depths of up to 100 μm. Excellent surface quality is achieved by initially protecting the optical surface with a sacrificial silicon dioxide layer that is later removed during chemical etching. To optimize cut quality and machining speed, we explored various laser machining parameters, including laser polarization, repetition rate, pulse duration, pulse energy, exposure time, and focusing, as well as scanning, protective coating, and etching procedures. The resulting structures significantly broaden the capabilities of terahertz polaritonics, in which lithium niobate and lithium tantalate are used for terahertz wave generation, imaging, and control. The approach should be applicable to a wide range of materials that are difficult to process by conventional methods.

Keywords femtosecond laser machining · hydrofluoric acid etch · lithium niobate · lithium tantalate · terahertz polaritonics · surface treatment · silicon dioxide · materials processing

Prasahnt Sivarajah · Christopher A. Werley · Benjamin Ofori-Okai · Keith A. Nelson
Department of Chemistry
Massachusetts Institute of Technology
77 Massachusetts Avenue, Cambridge, MA 02139
Tel: 6172531956
E-mail: kanelson@mit.edu

Christopher A. Werley
Department of Chemistry and Chemical Biology
Harvard University
12 Oxford Street, Cambridge, MA 02138 USA

1 Introduction

Lithium niobate ($LiNbO_3$, LN) and lithium tantalate ($LiTaO_3$, LT) have important roles in optics due to their nonlinear optical properties [1] . They have strong electro-optic, piezoelectric, and acousto-optic responses, making them valuable materials in a large variety of devices and experiments relating to the interactions among fields, light, and sound [2,3]. One important application in recent years has been efficient generation of terahertz (THz) frequency phonon-polariton waves — admixtures of polar lattice vibrations and electromagnetic radiation — by femtosecond optical pulses via the nonlinear process of impulsive stimulated Raman scattering (ISRS) [4–6]. This led to the development of the THz polaritonics platform, in which the THz waveform generated in $LiNbO_3$ or $LiTaO_3$ can be flexibly tuned and controlled [7–9]. In a $LiNbO_3$ or $LiTaO_3$ slab, the complete spatial and temporal evolution of the THz electric field can be recorded with time-resolved phase-sensitive imaging, yielding detailed insights into THz generation and interaction with a wide range of photonic, or "polaritonic," elements [10–15]. Since all of this takes place on a single chip, the polaritonics platform is compact, versatile, and easily integrated with other photonic systems, for example an optical modulator [16]. In an important recent application, generation and coherent superposition of polariton waves in bulk $LiNbO_3$ by spatially and temporally tailored optical pulses ("tilted pulse fronts") and coupling of the waves out of the $LiNbO_3$ crystal has yielded high-energy THz pulses now used widely for tabletop nonlinear THz spectroscopy and coherent control [17].

In polaritonics, THz waves can be manipulated by fabricated structures in slab waveguides that result in focusing [7], diffraction [18,19], additional waveguiding [20], filtering [21,22], localization and enhancement [23], or other specified transformations [24,21,25].

Critical to many of these applications is the ability to cut high-quality structures into the $LiNbO_3$/$LiTaO_3$ slab without degrading the waveguide surface, which must be of optical quality for optical imaging of the THz waves. In this paper we describe the optimization of such a fabrication procedure, which uses both femtosecond laser machining and chemical etching.

When searching for the most effective fabrication procedure for $LiNbO_3$ slabs, we first considered optical lithography, which has been highly refined for the integrated circuit industry [26]. However, using this technique to pattern structures in $LiNbO_3$ with thicknesses in the range of 10-100 μm is cumbersome and difficult. The materials are chemically very inert and resistant to etching of any kind, and even if an appropriate solvent could be found there is no reliable method to chemically etch such thicknesses [27,28]. On the other end of the spectrum, mechanical machining makes cutting structures in metals on the 100 μm length scale routine, but cutting 10 μm holes in thin, brittle substrates is extremely challenging. Still other techniques such as ultraviolet, sub-bandgap cw [29], and pulsed laser ablation are apt for the feature sizes required, but typically produce surface damage deleterious to waveguide performance necessary in THz polaritonics because a large fluence is required to pattern beyond a thickness of 5 μm [30,31]. The method that has proved to be best suited for producing the desired features in hard transparent materials is femtosecond laser machining. It was first demonstrated in 1994 in fused silica and metal films [32]; since then, it has been widely used in photonics and optics [33–37]. A focused femtosecond laser pulse with sufficient energy induces a structural change in the focal volume leading to a permanent change in the refractive index, and at even higher pulse energies ablation occurs. Although the effects of the ejected debris, or plume, can affect the ablation rate and must be considered at short delay times ($\sim$10s of ps for $LiNbO_3$) [38], it is possible to use femtosecond laser machining to cut a hole spanning the entire thickness of the material [39]. Laser machining has the advantage that no mask is required so it can be carried out through a direct-write process, making it more suitable than many typical top-down lithographic techniques [33,40, 41].

To create the structures required for THz polaritonics (dimensions on the order of $\lambda/2$ or 50 μm), it is difficult to ablate the entire pattern. As a result, we utilized the procedure of carving out the desired structure by tracing its outer boundary with the focused laser pulse, allowing the structure to simply detach and fall out. In fact, such femtosecond laser machining methods for patterning $LiNbO_3$ and $LiTaO_3$ slabs for THz polaritonics have been studied previously [21,24], but many densely packed structures could not be produced cleanly. There are two particularly challenging requirements for polaritonics samples: the surface must be maintained at high optical quality, and the damage and bevel of the cut surface must be minimized. Maintaining the optical-quality surfaces required for imaging of THz waves [13,24] is quite difficult due to redeposition of laser-ablated material. To address this problem, we deposited a protective layer of silicon dioxide (SiO_2) on the surface prior to laser machining and removed the coating, along with accumulated debris, with a post machining hydrofluoric acid (HF) etch. To minimize surface damage and bevel, which can adversely affect the performance of resonant cavities, waveguides, and other photonic elements as well as obscure some regions of the crystal during imaging, we carefully optimized many laser-machining parameters. We found that the bevel — which results from the conical shaped profile of a Gaussian beam before or after a focus — can be minimized by reducing the pulse energy to just above the damage threshold and tracing the desired pattern repeatedly at multiple sample depths. Machining in this manner yields structures with bevels approximately 2 μm wide, with further sharpening and cleaning of the features occurring during the chemical etching step. In the following sections, we discuss in detail the protective layer, optimized laser machining parameters, and chemical etching process. We demonstrate the fabrication capabilities by producing photonic crystal structures consisting of periodic arrays of holes cut through the crystal slabs. These are challenging patterns because of the small feature sizes and high feature density, so they serve as useful illustrations of the efficacy of our fabrication procedure.

2 Experimental Setup

The machining laser was an amplified Ti:Sapphire laser (800 nm central wavelength, 200 fs pulse duration, 1 kHz repetition rate, 6 μJ/pulse). Key optical components included a spatial filter to improve the spot quality, a shutter to block the laser when moving from one machining region to the next, and a waveplate-polarizer combination to control the power (see Fig. 1). The sample was mounted on an *xyz*-translation stage equipped with computer-controlled Newport LTA-HL motorized actuators with resolution of 0.05 μm and bi-directional repeatability of ± 1 μm, which enabled patterning of the crystal on the micron scale. The 800 nm pulse from the laser was directed onto the sample through a 0.25 numerical aperture (NA) objective, which caused ablation of the material at the focus via nonlinear absorption processes, the details of which are described in [41]. By focusing the laser at multiple depths spanning from the front to back of the sample, a clear hole can be cut through the entire thickness of the crystal; in our experiments the minimum diameter of the clear hole was 3 μm. Incoherent 532 nm light illuminated the sample, which was imaged onto a CCD camera using a 10 cm focal length lens that provided a depth of

focus of 30 μm, a resolution of 4 μm, and a magnification of 4; this enabled real-time monitoring of the machining as it occurred.

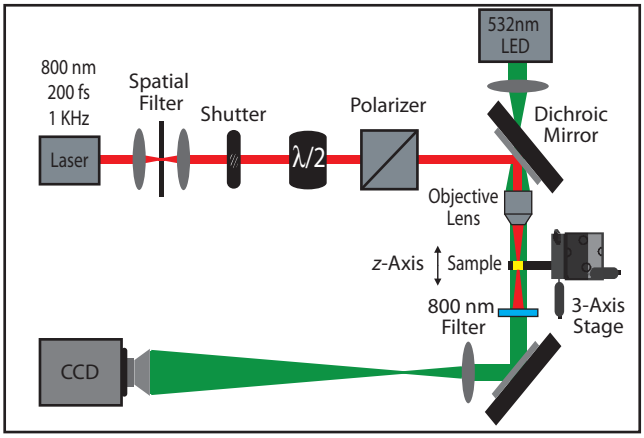

Fig. 1 The experimental laser machining setup where laser light is directed through a 0.25 NA objective onto a $LiNbO_3$ or $LiTaO_3$ sample. The laser beam spatial mode was improved with a spatial filter, while a waveplate-polarizer combination controlled pulse energy. A motorized actuator moved the sample relative to the focal spot in order to create the desired pattern, while a shutter controlled the exposure time. The sample was illuminated with incoherent 532 nm light and monitored in real time using a 1-lens imaging system

One experimental consideration is the method of sample exposure. Conventionally, polaritonics laser machining experiments have been done with a specified exposure time per point (by opening and closing a shutter for a specified interval of time), followed by moving to another point and re-exposing [21,24]. However, in order to create larger dimension structures that have been cleared throughout the thickness of the crystal, it is advantageous to keep the shutter open and perform a continuous cut as it greatly reduces the total time required to cut the structure and the wear on the shutter.

Another more crucial experimental consideration is that the crystal surface must be kept precisely perpendicular to the direction of beam propagation. Even a slight misalignment of the angle between the slab and the focal plane of the incoming beam leads to significant degradation in feature quality when moving from one side of a millimeter scale structure to another. The bevel increases significantly when the sample is translated only 15-20 μm out of the focal plane. To overcome this issue, we attached the sample to a mount with micrometer control over the crystal tilt. We first determined the z-position of 3 corners of the crystal by cutting holes in each. We then calculated and made the micrometer adjustments necessary to bring the entire crystal into the focal plane of the objective

3 Details of Optimized Parameters

In order to create a hole, laser machining was used to carve out a pattern defining the boundary of the circle, allowing the hole to fall out. In the process, the shutter was opened and the crystal was continuously exposed at every 2.5 μm along the circumference of the circle (each exposure herein referred to as a point) by using the motion controller to move the crystal slab laterally relative to the focus (coordinates of trace relayed by LabVIEW®) at a speed of 2.5 μm/ms. The shutter was opened to initialize tracing of the pattern and was closed when the pattern was traced out a specified number of times at successive z-depths. The stage then moved the crystal to a new set of coordinates, after which the shutter re-opened to trace out and cut the next structure.

There are a number of factors important in the machining procedure that must be considered to render optical quality surfaces, structures with a minimal bevel, and high resolution: protecting the surface from debris during machining, etching of the material, laser repetition rate, pulse energy, relative position of the crystal with respect to the focus (henceforth referred to as z-depth), exposure time, pulse duration, polarization, and sample frame used. These will be outlined in detail below. We first discuss surface coating and etching procedures that produce a clean surface and then examine laser characteristics and machining protocol that produce sharp features.

3.1 Surface Protection

For THz polaritonics and many other laser machining applications in dielectric crystals, semiconductors, metals, etc, optical surface quality is required. Typically, the surface quality deteriorates during laser machining because a significant fraction of the ablated material is redeposited on the surface of the crystal [42–44]. The redeposited material contains a number of highly reactive atomic, ionic, and molecular species. In $LiNbO_3$ they include Li^+, Nb^+, NbO^+, and triatomic NbO_2 and $LiO_2{}^+$ [45]. These react with and are chemically bonded to the otherwise clean surface and cannot be removed by a solvent that does not etch the crystal itself. This debris collects on both surfaces, but is more prevalent on the back where material is ablated when the hole breaks through.

In order to solve the problem of redeposited material, a number of techniques have been attempted in the past. These include solvent washes, protective sacrificial layers, air/nitrogen gas flowing by the sample surface during machining to blow away debris, machining in vacuum, and machining under fast flowing water films [46]. We did not attempt machining in vacuum or under water, but we did try many of the other methods. The redeposited material was impervious to a variety of organic solvents, strong acids, and

Piranha (1:3 H_2O_2:HNO_3). Flowing air across the sample had no noticeable effect. We also tried applying a protective polymer coating to the surface. Unfortunately, both polymethyl methacrylate (PMMA) and polyvinyl alcohol (PVA) coatings made the redeposition problem worse. The polymers, which were presumably hardened and crosslinked by the reactive ion species from the laser plasma, were resistant to a host of organic solvents, strong acids, and Piranha.

To overcome this issue it was necessary to choose a more chemically inert protective coating, one that is fully oxidized and can withstand the reactivity of the ablated species. In this vein, we chose 1 μm thick SiO_2 [47] to coat both surfaces of the crystal. There are multiple advantages to using SiO_2 as a coating: it is resistant to the ablated species and so protects the crystal underneath, it is thin and transparent so real-time imaging of the machining process is still possible, and it can be selectively etched and removed without impacting the unmachined portions of the substrate. We discuss the cleaning procedure fully in the following section.

3.2 Chemically Assisted Cleaning and Etching

The utilization of a HF etch in conjunction with SiO_2 provided a two-fold advantage. First, it etched away the protective SiO_2 coating, leaving a nearly pristine surface free of redeposited material. The etch times in HF solution were 30-40 minutes at room temperature, consistent with typical SiO_2 etch rates of 87 nm/min [48]. Under these conditions the optical quality of the unexposed surface was unaffected by the HF. A second benefit of the cleaning was that the HF etched and removed material from the regions that had been ablated at a considerably faster rate than it etched the unexposed crystal, thereby aiding in clearing debris from cuts in the sample.

Previous work has suggested that it is not possible to pattern thick ($>$10 μm) hard dielectric crystals using unassisted chemical etching alone [21,49,30,31]. This may be true for single crystals (etch rate of $<$2 nm/min for crystalline $LiNbO_3$), but amorphous material can be dissolved more than 1000 times faster (etch rate of $>$5 μm/min for amorphous $LiNbO_3$) [50]. We have exploited this by using laser machining to create an amorphous solid rather than removing the solid entirely by ablation. In this process, the initial laser shot removes a large portion of the material locally, and some of this material is redeposited on the surface. Subsequent shots ablate material deeper in the crystal, which gets deposited on the sidewalls or coagulates as a result of heating and ultimately recloses the void; this has been observed with as few as 5 laser pulses [49]. As opposed to further exposing the crystal until all material has been removed, we rely on the HF to complete the removal of the material without damaging the unexposed surface [see Fig. 2]. As a result, we avoid adversely affecting cut quality

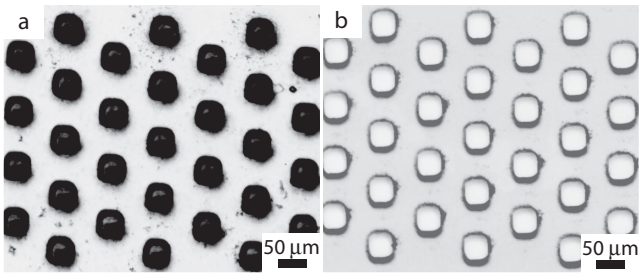

Fig. 2 Optical microscope images of a femtosecond laser-machined 54 μm thick slab of lithium tantalate, with a 1 μm silicon dioxide coating on both front and back surfaces. The hole diameter is 50 μm and the triangular lattice periodicity is 100 μm. (a) The sample immediately after laser machining. (b) The sample after an HF etch (1:5 HF:H_2O) for 30 minutes at room temperature, showing a clean surface and clear holes

at higher pulse energies as well as long exposure times required for complete ablation at lower pulse energies. In this way, the process takes advantage of both laser machining and chemical etching and has a resolution higher than the one from a conventional laser exposure method [21]. The result of utilizing a SiO_2 coating and HF etching is shown in Fig. 2, with excellent optical quality when imaged with a transmission microscope.

3.3 Laser Repetition Rate

The repetition rate of the femtosecond laser is important when machining dielectric materials. We initially attempted to machine $LiNbO_3$ slabs using a 250 kHz repetition rate, reasoning that many low-energy pulses would be able to cut very fine features. In fact, we observed severe sample cracking at pulse energies as low as 3 μJ, likely due to the thermal load exceeding the thermal dissipation rate [51]. When the power was reduced sufficiently to avoid cracking, exposure times became very long and there was significant degradation of surface quality. To address these issues, we moved to a 1 kHz repetition rate (Δt =1 ms) at which we found that sample cracking was rarely an issue, and the number of pulses was greatly reduced to minimize nearby surface damage.

3.4 Pulse Energy

Controlling the pulse energy is necessary to create the smallest damage spot size, while still creating enough damage such that the HF etch will clear the structure through the slabs thickness. We tested a wide range of pulse energies, and found the optimal energy for our focusing parameters to be roughly 6 μJ. Greater pulse energies led to unwanted damage, while smaller energies yielded minimal improvement in resolution with significantly longer scan times required to clear the hole. With 6 μJ/pulse, we cut a hole of

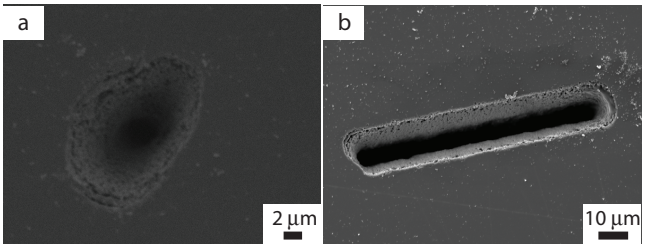

Fig. 3 SEM images of features produced in a 54 μm thick slab of lithium niobate with a 1 μm silicon dioxide coating on both front and back surfaces. These demonstrate the resolution of laser machining with a 0.25 NA and subsequent HF etching for 30 minutes at room temperature. (a) Hole with a diameter of 3 μm. (b) Line with width of 6 μm

only $\sim$3 μm in diameter and a line $\sim$6 μm in width through a 50 μm thick crystal slab utilizing the HF assisted method as shown in Fig. 3.

3.5 *Z*-Depth Scanning Range

The other major parameter of importance is the z-depth scanning range. In previous work [21], a lower NA lens was used in order to maintain a depth of focus (DOF) comparable to the crystal thickness such that a hole was cleared through the entire crystal thickness with the sample at a single z-depth, typically with the crystal center at the focal plane. The disadvantage of the lower-NA lens choice is that the resolution scales with the inverse of NA, so the feature size is increased when moving to a larger DOF. In order to preserve high lateral resolution we used a higher NA lens (0.25), but the smaller DOF made it necessary to move the focus relative to the sample (along the z-axis) and cut the pattern at multiple depths within the crystal to fully clear out the hole. Thicker crystals required more cuts at more z-depths.

We found that for the 0.25 NA lens (DOF = 8 μm), the optimal step size between traces was $\Delta z \approx 16\mu m \approx 2 \cdot \mathrm{DOF}$. When larger steps were taken along z, the pulse energy had to be increased to fully cut through the sample, resulting in more damage around the cut. Smaller steps along z led to a negligible reduction in bevel but required significantly longer scan times and led to increased material redeposition on the crystal surface. In a 54 μm thick crystal, we achieved a 2 μm bevel from the front to back surface, only slightly larger than the diffraction-limited spot [$\lambda/(2\mathrm{NA}) = 1.6$ μm]. The bevel was measured by comparing the radius of the patterned holes on both the front and backside of the crystal (see Fig. 4 (a),(b)), and SEM images of the sidewall confirmed this slanted profile (see Fig. 4 (c)).

Fig. 4 (d), which is a representative example of experiments used to optimize the experimental parameters we discuss, shows 50 μm diameter holes patterned at a succession of pulse energies and z-depths followed by etching in an HF

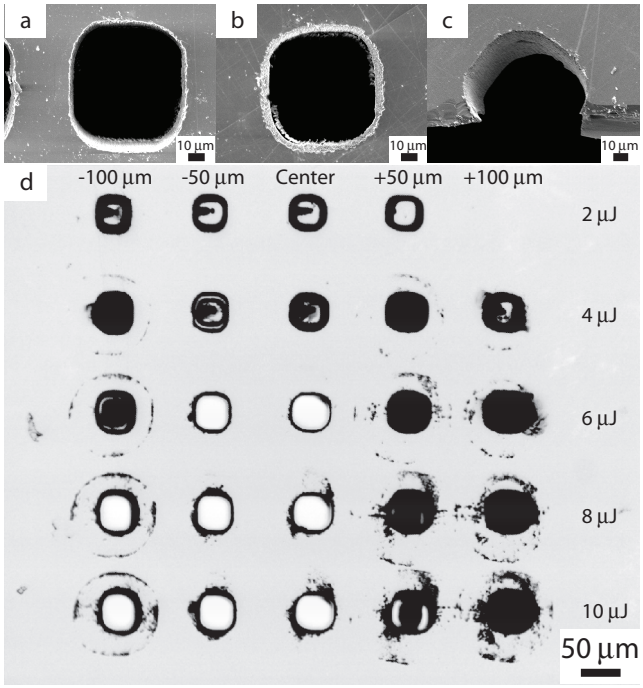

Fig. 4 Images of holes machined on a 54 μm $LiNbO_3$ sample using a 0.25 NA objective and subsequent HF etching for 30 minutes at room temperature. (a) SEM image of the front of a single machined hole with diameter of $\sim$69.7 μm. (b) SEM image of the back of the crystal with diameter of $\sim$65.7 μm, together with (a) demonstrating a 2 μm bevel at optimum machining conditions (c) SEM image of the sidewall of a hole with diameter of $\sim$80 μm demonstrating minimal sidewall roughness and a slightly slanted profile from front to back (d) Optical microscope image of 50 μm diameter holes created to analyze influence of laser pulse energy (indicated on the right) and z-depth (indicated across the top). "Center" indicates the focal plane at the center of the 54 μm crystal thickness. Positive z-depth values indicate the focal plane closer to the front surface of the crystal, negative values closer to the back surface. Each of the values indicates the center about which four machining scans were conducted at 16 μm intervals

bath (1:5 HF:H_2O). Four repetitions at 16 μm z-depth increments were used to create an air hole structure with the z-position in the figure referring to the center position for that set of scans. Note that for the 2 and 4 μJ pulse energies, the un-machined portion of the $LiNbO_3$ crystal inside the circle, which was supposed to fall out during the machining or subsequent etching, is still visible because the cut did not fully penetrate the slab. Further, it is clear that both alignments relative to focus and pulse energy have large effects on the damage profile. Care is required to obtain high quality features.

3.6 Exposure Time

Having determined the optimal z-depth increment, it was then important to minimize the exposure time during each machining scan. This parameter can be labeled more appropriately as "pulses per point per repetition" in our process

due to the re-tracing at multiple z-depths. After the material in the laser focus has been ablated, exposing for more time has very little effect except for some deleterious redeposition of waste on the crystal surface. For this reason, and to minimize overall fabrication time, we determined the minimal number of pulses required to create enough damage such that an HF etch could clear out the hole. The result was approximately 5 pulses per point per repetition. A 54 μm thick sample of $LiNbO_3$/$LiTaO_3$, where the z-scan parameter dictates re-tracing the same pattern at 4 depths, requires a total of 20 pulses at 6 μJ for each (x,y) location in a machined sample structure. For the circular structures in this paper, 90 points along the circumference of the hole were used to carve the pattern, which translates to a total of 1800 pulses to create a structure. This is much reduced from previous work where roughly five thousand 10 μJ pulses at 800 nm were required to reach a penetration depth of 50 μm [21], clearly showing the advantage of scanning the z-depth and using the HF etch to help clear the hole.

3.7 Pulse Duration and Polarization

We investigated several other parameters in order to gauge their influence on the quality of laser machining, most notable of which were pulse duration and polarization. The laser pulse was stretched from 200 fs to 1.2 ps, which had minimal impact on machined structure quality. The polarization state of the cutting laser (circular, vertical, and horizontal polarizations relative to the optic axis of the x-cut crystals were tried) also had minimal impact.

3.8 Sample Frame

When dealing with such brittle crystals, only tens of microns thick, mounting of the sample in a rigid frame during processing and subsequent experiments greatly increases the chances that the sample will survive unbroken. Since the z-position of the sample has been determined to be sensitive within 16 μm, it is also important that the frame/holder used to mount the crystal be made of a fairly smooth material that allows level placement of the sample. We had good results with a frame made from a $\sim$1 mm thick piece of nickel (Alloy 400), which is rigid and smooth, can be easily machined on a standard mill, and is impervious to the HF etch. The crystal slab can be easily and reversibly attached to the frame using a clear base coat nail polish (such as Maybelline - Express Finish® 50 Second), which also withstands the HF etch.

4 Results and Summary

Fig. 5 (a) and (b) show two extended structures fabricated in lithium tantalate using all the optimized parameters discussed in section 3. The structures are photonic crystals, periodic arrays of holes used to create band gaps (frequency ranges where light is not allowed to propagate) and to otherwise modify light dispersion. These are particularly difficult to fabricate because they are made of many small, closely spaced structures that produce a great deal of debris and that present a significant risk of sample cracking. As is evident from the figure, the machining procedure described can create very fine features over large areas without degrading surface quality. The field of view for the structures shown is 3 mm, but we have machined structures as large as 1 cm in length. In principle, the size of the structures is only limited by the sample size and the range of travel of the motorized actuators.

The ability to image THz electric fields within such cleanly machined, optical quality structures is demonstrated in Fig. 5 (c). This is one frame from a movie of THz electric fields travelling at the speed of light and interacting with the photonic crystal lattice. The frame was recorded with a probe pulse that was delayed by 40 ps following a pump pulse that generated a THz wave that propagated at light-like speeds in the $LiNbO_3$ slab waveguide. Phase-sensitive imaging was used to visualize the spatially varying transmitted probe light intensity I(x,y), whose polarization was rotated by the THz field [52]. A reference image $I_o(x,y)$ was recorded with the pump pulse blocked and the THz field absent. The image shows the THz-induced change in signal, calculated as [$I(x,y)$ - $I_o(x,y)$] / $I_o(x,y)$. Many additional images were recorded with different pump-probe delay times, and played in rapid succession they present a "movie" of THz wave propagation in the machined crystal, permitting close observation of the field within a photonic bandgap structure.

To summarize the important parameters discussed above, a typical machining procedure is outlined here for cutting holes in a crystal slab 50 μm thick, in this case x-cut lithium tantalate. To begin, the process involves a plasma enhanced chemical vapor deposition (PECVD) step to coat both sides of the sample with a 1 μm layer of SiO_2. After coating, the sample is mounted on the nickel frame as described above. Following this, the sample is oriented with the plane perpendicular to the beam direction, and laser machining is done on the sample at 4 depths with a z-depth scanning increment of 16 μm (e.g. front surface, 16 μm, 32 μm, back surface) using the experimental setup shown in Fig. 1. Pulse energy for the system is kept to 5-6 μJ/pulse with 5 pulses per point per repetition. This is followed by an HF etch of the sample (1:5 HF:H_2O) for 30-40 minutes, which preferentially etches the transformed material and protective silica coating, resulting in a clean surface and in holes cleared through the thickness

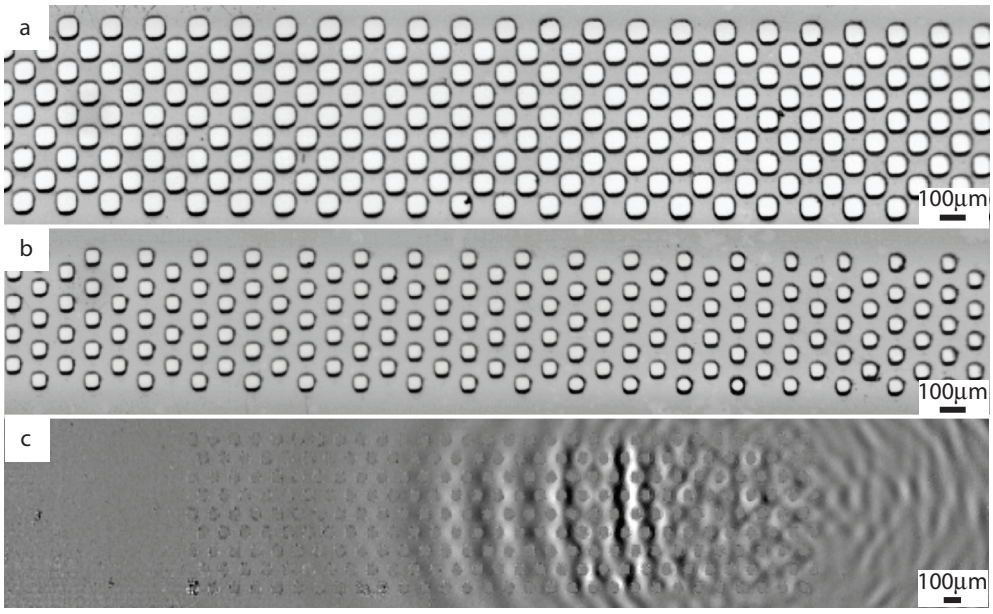

Fig. 5 Images of large-scale features created in a 54 μm $LiTaO_3$. (a) A square lattice of air holes, rotated by 45^o, with a diameter of 70 μm and a 100 μm periodicity. (b) A triangular lattice of air holes with a diameter of 50 μm and 100 μm periodicity. In (a) and (b), the total field of view is 3 mm and imaging was done with an optical microscope. (c) Image of THz field in a hexagonal lattice of 100 μm periodicity and 25 μm hole radius

Table 1 Optimized parameters for laser machining of $LiNb_3/LiTaO_3$

Parameter	**Optimized Value**
Pulses per point per z-depth	5
Pulse energy	6 μJ
Laser repetition rate	1 kHz
z-depth scanning increment	16 μm
Surface coating	1 μm SiO_2
HF etch time (1:5 HF:H_2O)	30-40 minutes
Pulse duration	Not critical (200 fs - 1.2 ps)
Polarization	Not critical
Optimal resolution	3 μm
Machinable area	>1 cm^2

of the crystal. For convenience, the important optimized parameters are outlined in Table 1.

5 Conclusion

We have demonstrated a novel process of $LiNbO_3/LiTaO_3$ fabrication that yields greater control than conventional optical lithography or previously demonstrated laser machining by combining optical and chemical processing. The HF etch removes a protective SiO_2 layer, yielding extremely clean surfaces. In addition, HF preferentially etches damaged material, reducing the bevel and increasing overall resolution.

During processing, it is important to consider the various critical parameters that must be controlled. Pulse energy and exposure time must be minimized to just above the damage threshold, followed by scanning along the z-axis in step sizes roughly double the depth of focus. This process allows subsequent HF etching to clear out the desired structure through the crystal thickness. These steps are utilized to protect the optical surface and minimize bevel, both crucial indicators of laser machining quality. It may be possible to achieve finer resolution in the future using a higher NA lens or shorter wavelength light to reduce the diffraction-limited spot size. Under some circumstances it might be possible to fabricate structural elements smaller than the diffraction limit, as has been demonstrated in some other laser machining processes [32,53].

The fabrication process was originally optimized for $LiNbO_3$. The same optimized parameters were then applied to $LiTaO_3$, another dielectric single crystal, with good results. This is an indication that the protocol we developed could be applied without major modification to an array of transparent materials.

Acknowledgements This work was supported by the National Science Foundation under grant no. ECCS-1128632. B. K. O. was supported in part by an NSF GRFP fellowship and P. S. was supported by a Canadian Research Fellowship. Furthermore, SiO_2 was deposited and etched at the Microsystems Technology Laboratories (MTL), and the crystals were characterized by SEM at the MIT Center for Materials Science and Engineering (CMSE). We thank both the staff of MTL and CMSE for their assistance, in particular Kurt Broderick for his insight and training.

References

1. K. Wong, *Properties of Lithium Niobate* (The Institution of Engineering and Technology, 2002)
2. L. Arizmendi, Phys. Status Solidi A. **201**(2), 253 (2004). DOI 10.1002/pssa.200303911. URL http://doi.wiley.com/10.1002/pssa.200303911
3. R.S. Weis, T.K. Gaylord, Appl Phys A Solid Surface **37**(4), 191 (1985)
4. D. Auston, M. Nuss, IEEE J. Quantum. Electron. **24**(2), 184 (1988)
5. T.P. Dougherty, G.P. Wiederrecht, K.A. Nelson, J. Opt. Soc. Am. B **9**(12), 2179 (1992)
6. K.L. Yeh, M.C. Hoffmann, J. Hebling, K.A. Nelson, Appl. Phys. Lett. **90**(17), 171121 (2007)
7. T. Feurer, J.C. Vaughan, K.A. Nelson, Science **299**(5605), 374 (2003)
8. D.W. Ward, E. Statz, J.D. Beers, N. Stoyanov, T. Feurer, R.M. Roth, R.M. Osgood, K.A. Nelson, eprint arXiv:cond-mat/0401049 (2004)
9. K.H. Lin, C.A. Werley, K.A. Nelson, Appl. Phys. Lett. **95**(10), 103304 (2009)
10. R.M. Koehl, S. Adachi, K.A. Nelson, J. Phys. Chem. A **103**(49), 10260 (1999)
11. P. Peier, S. Pilz, F. Müller, K.A. Nelson, T. Feurer, J. Opt. Soc. Am. B **25**(7), B70 (2008)
12. H. Inoue, K. Katayama, Q. Shen, T. Toyoda, K.A. Nelson, J. Appl. Phys. **105**(5), 054902 (2009)
13. Q. Wu, C.A. Werley, K.H. Lin, A. Dorn, M.G. Bawendi, K.A. Nelson, Opt. Express **17**(11), 9219 (2009)
14. C. Yang, Q. Wu, J. Xu, K.A. Nelson, C.A. Werley, Opt. Express **18**(25), 26351 (2010)
15. C.A. Werley, Q. Wu, K.H. Lin, C.R. Tait, A. Dorn, K.A. Nelson, J. Opt. Soc. Am. B **27**(11), 2350 (2010)
16. E. Wooten, K. Kissa, A. Yi-Yan, E. Murphy, D. Lafaw, P. Hallemeier, D. Maack, D. Attanasio, D. Fritz, G. McBrien, D. Bossi, IEEE J. Sel. Topics in Quantum Electron. **6**(1), 69 (2000)
17. J. Hebling, K.L. Yeh, M.C. Hoffmann, B. Bartal, K.A. Nelson, J. Opt. Soc. Am. B **25**(7), B6 (2008)
18. N.S. Stoyanov, T. Feurer, D.W. Ward, K.A. Nelson, Appl. Phys. Lett. **82**(5), 674 (2003)
19. C.A. Werley, K.A. Nelson, C. Ryan Tait, Am J Phys **80**(1), 72 (2012)
20. N.S. Stoyanov, D.W. Ward, T. Feurer, K.A. Nelson, Nat. Mater. **1**(2), 95 (2002)
21. D. Ward, E. Statz, K. Nelson, Appl. Phys. A: Mater. Sci. Process. **86**(1), 49 (2006)
22. P. Peier, S. Pilz, T. Feurer, J. Opt. Soc. Am. B **26**(8), 1649 (2009)
23. C.A. Werley, K. Fan, A.C. Strikwerda, S.M. Teo, X. Zhang, R.D. Averitt, K.A. Nelson, Opt. Express **20**(8), 8551 (2012)
24. P. Peier, H. Merbold, V. Pahinin, K.A. Nelson, T. Feurer, New J. Phys. **12**(1), 013014 (2010)
25. D.W. Ward, J.D. Beers, T. Feurer, E.R. Statz, N.S. Stoyanov, K.A. Nelson, Opt. Express **29**(22), 2671 (2004)
26. B. Fay, Microelectron. Eng. **61-62**(null), 11 (2002)
27. F. Laurell, J. Webjorn, G. Arvidsson, J. Holmberg, J. Lightwave Technol. **10**(11), 1606 (1992)
28. I.E. Barry, G.W. Ross, P.G. Smith, R.W. Eason, G. Cook, Mater. Lett. **37**(4-5), 246 (1998)
29. F.K. Christensen, M. Mullenborn, Appl. Phys. Lett. **66**(21), 2772 (1995)
30. P. Brown, Opt. Mater. **20**(2), 125 (2002)
31. S. Mailis, C. Sones, J. Scott, R. Eason, Appl. Surf. Sci. **247**(1-4), 497 (2005)
32. P. Pronko, S. Dutta, J. Squier, J. Rudd, D. Du, G. Mourou, Opt. Commun. **114**(1-2), 106 (1995)
33. R.R. Gattass, E. Mazur, Nat. Photonics **2**(4), 219 (2008)
34. F. Korte, J. Serbin, J. Koch, A. Egbert, C. Fallnich, A. Ostendorf, B.N. Chichkov, Appl. Phys. A: Mater. Sci. Process. **77**(2), 229 (2003)
35. A. Zoubir, L. Shah, K. Richardson, M. Richardson, Appl. Phys. A: Mater. Sci. Process. **77**(2), 311 (2003)
36. L. Shah, A.Y. Arai, S.M. Eaton, P.R. Herman, Opt. Express **13**(6), 1999 (2005)
37. A.M. Kowalevicz, V. Sharma, E.P. Ippen, J.G. Fujimoto, K. Minoshima, Opt. Express **30**(9), 1060 (2005)
38. S. Preuss, M. Spath, Y. Zhang, M. Stuke, Applied Physics Letters **62**(23), 3049 (1993)
39. C. Schaffer, J. García, E. Mazur, Appl. Phys. A: Mater. Sci. Process. **76**(3), 351 (2003)
40. J. Meijer, K. Du, A. Gillner, D. Hoffmann, V. Kovalenko, T. Masuzawa, A. Ostendorf, R. Poprawe, W. Schulz, CIRP Ann. Manuf. Technol. **51**(2), 531 (2002)
41. X. Liu, D. Du, G. Mourou, IEEE J. Quantum. Electron. **33**(10), 1706 (1997)
42. F. Meriche, E. Neissclauss, R. Kremer, A. Boudrioua, E. Dogheche, E. Fogarassy, R. Mouras, A. Bouabellou, Appl. Surf. Sci. **254**(4), 1327 (2007)
43. S. Preuss, A. Demchuk, M. Stuke, Appl. Phys. A: Mater. Sci. Process. **61**(1), 33 (1995)
44. A. Serafetinides, C. Skordoulis, M. Makropoulou, A. Kar, Appl. Surf. Sci. **135**(1-4), 276 (1998)
45. M. Affatigato, K. Tang, R.F. Haglund, C.H. Chen, Appl. Phys. Lett. **65**(14), 1751 (1994)
46. T. Mai. Toward debris-free laser micromachining - Industrial Laser Solutions (2008)
47. H.W. Chong, A. Mitchell, J.P. Hayes, M.W. Austin, Appl. Surf. Sci. **201**(1-4), 196 (2002)
48. K. Williams, R. Muller, J. Microelectromech. Syst. **5**(4), 256 (1996)
49. A. Malshe, D. Deshpande, E. Stach, K. Rajurkar, D. Alexander, CIRP Ann. Manuf. Technol. **53**(1), 187 (2004)
50. L. McCaughan, T.F. Kuech, D.A. Saulys, V.A. Joshkin, A. Chowdhury, C.M. Staus. United States Patent: 6545791 (2002)
51. S.M. Eaton, H. Zhang, P.R. Herman, F. Yoshino, L. Shah, J. Bovatsek, A.Y. Arai, Opt. Express **13**(12), 4708 (2005)
52. C.a. Werley, S.M. Teo, B.K. Ofori-Okai, P. Sivarajah, K.a. Nelson, IEEE Trans. Terahertz Sci. Technol. **3**(3), 239 (2013)
53. F. Korte, S. Adams, A. Egbert, C. Fallnich, A. Ostendorf, S. Nolte, M. Will, J.P. Ruske, B. Chichkov, A. Tuennermann, Opt. Express **7**(2), 41 (2000)